PREDICTIONS OF SOLID-STATE HYDROGEN STORAGE SYSTEM CONTAMINATION PROCESSES

Dedrick, D.E.[1], Kanouff, M.P., Larson, R.S., and Bradshaw, R.W., Graetz, J., Hwang, S.
[1] Thermal/Fluids Sci. Eng., Sandia National Labs, P.O. Box 969, Livermore, CA, 94551, USA,
dededri@sandia.gov

ABSTRACT

Solid state materials such as metal and chemical hydrides have been proposed and developed for high energy density automotive hydrogen storage applications. As these materials are implemented into hydrogen storage systems, developers must understand their behavior during accident scenarios or contaminated refueling events. An ability to predict thermal and chemical processes during contamination allows for the design of safe and effective hydrogen storage systems along with the development of appropriate codes and standards. A model for the transport of gases within an arbitrary-geometry, reactive metal hydride bed (alane, α-AlH$_3$) is presented in this paper. We have coupled appropriate Knudsen-regime permeability models for flow through packed beds with the fundamental heat transfer and chemical kinetic processes occurring at the particle level. Using experimental measurement to determine and validate model parameters, we have developed a robust numerical model that can be utilized to predict processes in arbitrary scaled-up geometries during scenarios such as breach-in-tank or contaminated refueling. Results are presented that indicate the progression of a reaction front through a compacted alane bed as a result of a leaky fitting. The rate of this progression can be limited by; 1) restricting the flow of reactants into the bed through densification, and 2) maximizing the rate of heat removal from the bed.

NOMENCLATURE

c	species concentration, mol/cm^3	M	molecular weight
c_p	heat capacity, J/g-K	p	pressure, atm
d	diameter, dimensionless	Q	Activation energy
$\mathcal{D}$	species diffusivity, cm^2/s	R	reaction rate, mol/cm^3-s
h_w	heat transfer coef., W/cm^2-K	ν	gas velocity, cm/s
H	enthalpy, J/g-K	ϕ	porosity, dimensionless
K	permeability, cm^2	μ	dynamic viscosity, g/cm-s
k	thermal conductivity, W/m-k	ρ	gas density, g/cm^3
Kn	Knudsen number, dimensionless	τ	tortuousity, dimensionless
k_x	pre-exponential rate parameter		

1.0 INTRODUCTION - METAL HYDRIDE SYSTEMS

Hydrogen storage technologies that are efficient, low cost, and robust must be developed to enable the use of hydrogen fuel in transportation applications. Current technologies for automotive hydrogen storage (liquid and compressed gas) do not satisfy energy density requirements and are unable to provide a pathway for additional efficiency improvement. Solid-phase hydrogen storage solutions, such as reversible metal hydrides, are theoretically able to store more hydrogen per unit volume than liquid or compressed gas storage systems [1]. Given this potential for high energy density hydrogen storage, an internationally-supported research and development effort has been undertaken to develop technologies based on solid-phase hydrogen storage materials [2].

In addition to the energy density performance requirements, the engineered system must be safe and appropriate for the consumer automotive environment. The automotive platform is a dynamic hydrogen storage application intrinsically subject to a highly variable environment, uncertain hydrogen refueling quality control, and accidents. The nature of this duty cycle increases the

likelihood that the storage materials or containment structures may be compromised during the lifetime of the hydrogen storage system. In an accident or contaminated refueling scenario, the hydrogen storage material may be exposed to air, water and other contamination. Due to the requirements for high energy density hydrogen storage solutions, materials comprised of light metal elements are of specific interest - including, but not limited to, lithium (Li), sodium (Na), magnesium (Mg), calcium (Ca), boron (B), and aluminum (Al). Hydrides and complexes synthesized from these elements are typically found in the form of finely divided powders that can be pyrophoric and water reactive. Furthermore, the oxidation reaction products may themselves present hazards.

In this paper, we assemble transport and chemical kinetic models that can accurately describe contamination reaction processes in reactive porous beds. We have validated our models by considering processes observed in a specific material, alane, a prototype reactive hydrogen storage medium. The following sections describe the models and validating experiments undertaken to understand the transport of gases through a porous medium and the reaction of those gases with a solid particle, followed by the transport of heat from the reaction site to the surrounding particle bed and wall. Coupling of these transport models resulted in a validated overall model capable of predicting accident scenarios in systems of arbitrary geometry. In this paper, we focus on the breach-in-tank contamination scenario identified as a potential failure mode associated with solid state hydrogen storage systems [3].

1.1 Alane as a Hydrogen Storage Material

Solid-state material hydrogen storage systems for vehicular applications can be broadly categorized into two distinct fueling cycles: on-board reversible and off-board regenerated. In on-board reversible systems, hydrogen storage is realized with materials that remain on-board the vehicle during the entire fueling cycle. A wide range of reversible metal hydrides can in principle be utilized as reversible metal hydrides for automotive applications including metal alloys that form interstitial bonds with hydrogen (such as Laves phase hydrides) and covalently bonded, ionic complexes (such as sodium alanates). Although attractive due to reversibility, these materials suffer from low gravimetric storage densities. To overcome this, researchers have considered other materials that contain much larger hydrogen content as measure by weight.

Alane (AlH_3) has been proposed as a hydrogen storage chemical due to its high hydrogen storage capacity (10.5 wt%), moderate hydrogen release temperatures (~150°C), and low enthalpy of hydrogen release (9.9 kJ/mol-AlH_3). Unfortunately, these attractive thermodynamic properties are accompanied by high equilibrium pressures, making a storage system based on alane effectively non-reversible at practical hydrogen over-pressures. Researchers are addressing reversibility through a variety of methods, including particle size, additives, and ionic liquid synthesis processes [4]. Large cuboids of alane were originally prepared by the Dow Chemical Co [5-7]; however, these materials demonstrate decomposition temperatures in excess of 150°C. Graetz and others at Brookhaven National Labs [8] have been synthesizing new materials with more appropriate properties for automotive applications, including lower hydrogen release temperatures. Alane along with its decomposition product aluminum, like many hydrogen storage materials of this class, is sensitive to contamination. Due to its relatively simple chemistries and limited number of potential reaction pathways, alane provides a unique opportunity to investigate processes experienced during contamination of systems containing reactive high-surface area materials.

1.2 Contamination Processes in Alane Systems

In the case of alanes, the process of aluminum oxide formation under exposure to oxygen from the ambient environment is of specific interest. The amount of energy involved in this process is significant assuming the complete dehydrogenation of the alane followed by the oxidation of aluminum. In this case we do not consider the oxidation of hydrogen. The process begins with the decomposition of AlH_3 to Al solid and H_2 gas,

$$AlH_3(s) \rightarrow Al(s) + \frac{3}{2}H_2(g)$$
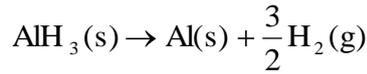
Eq. 1

In the presence of air, oxygen gas presumably diffuses into the solid particle and forms aluminum oxide

$$Al + \frac{3}{2}O(s) \rightarrow \frac{1}{2}Al_2O_3$$
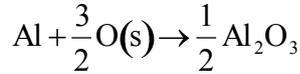
Eq. 2

If this process is not controlled, excessive heat can lead to combustion and/or failure of the containment vessel and present a hazard to the surrounding personnel. It should be noted that very few studies of alane oxidation have been reported in the literature. Past studies have focused on processes taking place in a combustion environment; in such cases, the consensus is that alane first releases hydrogen and then reacts at high temperature to form molten Al_2O_3 [9, 10] Work on the interaction of alane with potential oxidizers at moderate temperatures appears to be nonexistent, so even the reaction products have not been verified. As will become clear from the experiments, we will be concerned only with the oxidation of aluminum at relatively low temperatures.

2.0 MODELING AND SIMULATION OF CONTAMINATION

2.1 Governing Equations

Modeling and simulation of processes within a reactive porous media bed require solving the momentum, energy, and species conservation equations. Momentum transport was calculated with the Brinkman equation and associated continuity equation:

$$\frac{\rho \partial v}{\partial t} + \frac{\mu}{K}v = -\nabla p + \nabla \cdot \left[\mu\left(\nabla v + \nabla v^T\right)\right] - \frac{2}{3}\nabla\left(\mu\nabla \cdot v\right)$$

Eq. 3

$$\frac{\partial \rho}{\partial t} + \nabla \cdot (\rho v) = MR$$

Eq. 4

where K is the permeability, v is the superficial velocity (or Darcy velocity) and ϕ is porosity. Molecular weight is designated as M and R is the reaction rate where gas (oxygen) is the reactant and the product is a solid (Al_2O_3). Note that the compressible form of the equations are used to capture the effect of large pressure and density variations in the gas as it flows through a hydride packed bed. The energy transport equation includes a chemical reaction source term, where ΔH is the enthalpy of reaction:

$$\left(\rho c_p\right)_m \frac{\partial T}{\partial t} + \left(\rho c_p\right)_g v \cdot \nabla T = k_m \nabla^2 T + R\Delta H$$

Eq. 5

There are multiple species present in the gas phase requiring solution of the species transport equation:

$$\frac{\partial c_i}{\partial t} + \nabla \cdot (v c_i) = \nabla \cdot (\phi \mathcal{D} \nabla c_i) + R_i$$

Eq. 6

2.2 Chemical Kinetics Model of Aluminum Oxidation

Due to the rapid formation of an aluminum shell on the surface of an alane particle during dehydrogenation, we chose to consider the oxidation of aluminum as the basis of our model. Experimentally, little difference is seen between the oxidation of Al versus AlH_3. The authors assume that this is most likely due to only the outer shell of Al participating in the reaction. A mathematical model for the low-temperature oxidation (as opposed to combustion) of a spherical aluminum particle has been developed. The model provides the functional relationship between the oxidation rate and

the extent of reaction (as well as temperature) in a bed of such particles. The development is based on the well-known shrinking-core model for heterogeneous consumption of a spherical particle, but an approximate analytical solution is obtained by exploiting the fact that the process essentially stops while the extent of reaction is still small. A key assumption in the single-particle oxidation model is that O_2 dissociates and dissolves at the outer surface of the particle, $O_2 \Leftrightarrow 2 \, O(s)$. The dissolved oxygen diffuses through the growing oxide layer and reacts with aluminum at the oxide-aluminum interface. Dissociation is assumed to be at equilibrium, and diffusion is taken to be pseudo-steady relative to the movement of the interfaces.

To obtain the bulk reaction rate for the case of thin oxide layers, the particle level model is combined with the mass balance equations for the motion of the interfaces. The bulk reaction rate, or the rate of change in the bulk aluminum concentration, takes the form

$$\frac{d[\text{Al}]}{dt} = -\frac{6(1-\phi)\sqrt{p}k_0 e^{-Q/RT}}{D}\left[1 - \frac{2 + \alpha D k_1 e^{Q_1/RT}}{3}\left(1 - \frac{[\text{Al}]}{[\text{Al}]_0}\right)\right] \qquad \text{Eq. 7}$$

where [Al] is the bulk aluminum concentration, ϕ is the initial porosity of the bed, p is the partial pressure of oxygen, D is the initial particle diameter, α is the metal to metal oxide density ratio, R is the gas constant, and T is the temperature. The kinetic parameters that are fit based on experimental data are k_0, k_1, Q, and Q_1, which are the pre-exponentials and activation energies, respectively. The term, k_1 incorporates the diffusivity of oxygen in the oxide layer, while k_0 incorporates the equilibrium constant for oxygen dissociation.

Experimentally, there is a positive correlation between the amplitude of the exotherm and increasing temperature, i.e., the spike becomes larger as the initial temperature increases. To verify that our model correctly represents this correlation, the plot below (Figure 1) shows numerical results for dimensionless temperature vs. time for a set of arbitrary parameters. The desired behavior is qualitatively reproduced. This shows that the model is capable of describing the basic features of the experimental results.
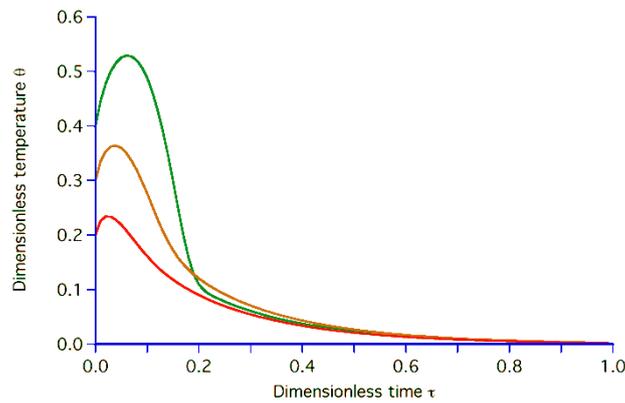

Figure 1. Plot demonstrates of the model sensitivity for a set of arbitrary parameters. A positive correlation is realized between the exotherm amplitude and increasing temperatures.

2.3   Models for transport properties

High surface area solid-phase hydrogen storage beds are frequently characterized by small particle sizes. These small particles lead to small pore sizes in the packed bed, which can result in large Knudsen numbers and transition into a slip flow regime. For this reason we use a permeability model

that includes Knudsen effects, as described by Young and Todd [11] that applies to continuum and rarefied flows:

$$K = \frac{\phi}{\tau^2} d_p^2 \left[\frac{1}{32} + \frac{5}{12} Kn \right],$$

Eq. 8

where d_p is the pore diameter and τ is the tortuosity. Porosity is determined through sample mass and volume measurements. There are two limitations to this model. First, in practice, hydride beds have a distribution of pore diameters, d_p. To address this, the pore diameter is treated as an experimental fit parameter and compared to SEM imaging analysis of the compacted bed. Secondly, the tortuosity, τ, is very difficult to measure and therefore it was inferred from experimental data.

In the absence of direct measurement, the thermal conductivities of the bed are estimated using established models in the absence of experimental measurement. The model utilized in this effort was developed by Zehner, Bauer, and Schlünder and reported in Tsotsas and adapted by Rodriguez-Sanchez [12]. The thermal conductivity, k_m, of an alane bed was estimated to vary between 0.1 and 1.0 W/m-K for void fractions ranging from 50 to 80% and hydrogen pressures up to 1 MPa. A value of 0.1 was utilized for most calculations.

A power law was used for the temperature dependent viscosity of air, μ (g/cm/s) = 0.0001716 $(T/273)^{0.666}$ [13]. A power law was also used to account for the temperature dependence of the diffusivity of oxygen in air, based on data reported by Mills [14], $\mathcal{D}$ (cm^2/s) = $0.325p^{-1}(T/400)^{1.701}$, where the pressure, p, is in atmospheres. The ideal gas law was used for the gas density. The density of the alane bed was measured (0.327 g/cc), and the specific heat of aluminum, c_p = 0.9 J/g/K, was used for the alane bed during oxidation, where it was assumed the alane dehydrogenated prior to oxidation.

3.0 MODEL PARAMETER CHARACTERIZATION

A small flow-through manifold was utilized to experimentally determine the permeability model parameters. A flow-through sample holder, shown in Figure 2, was developed to constrain a sample of alane between two frits. A heater wrapped around the sample holder was used to control temperature. A flow-through gas manifold was used to quantify the pressure drop across the sample. The samples were loaded at a density of 0.33 g/cc or approximately 23% dense. Figure 3 shows the model geometry and calculated helium pressure distribution in the sample holder with the frits and sodium alanate present. This model (along with a second version in which the sample was absent) was used to determine the parameters for the permeability model for both the alane and the frits. The model was assembled using Comsol™ Multiphysics.

3.1   Permeability Model Parameters

Prior to applying the momentum transport calculations to reactive bed predictions, validation experiments were completed to gain confidence in the permeability models. We characterized the flow through stainless steel frits of different grades (Mott Corporation grade 2 and 0.2) by measuring the pressure drop as a function of gas species, flow rate, temperature, and average pressure. The two grades produced a range of Knudsen flow characteristics that are of similar pore geometry as can be expected in a compacted metal hydride bed. The model accurately represented the pressure drop for a range of nitrogen and helium flow rates and pressures.

After gaining confidence in the model with a well characterized material, the parameters were determined for the flow field within packed alane beds. Using the pressure drop data, pore diameters ranging from 1.6 to 2.7 μm were calculated for a variety of beds ranging from 20 to 32% dense. This range of pores falls in line with estimations acquired from Scanning Electron Micrographs (SEM) of

the packed bed shown in Figure 5. The permeabilities resulting from these pore diameters ranged from 1.6 to 5.5 µm2. Tortuosity was estimated to have a value of 2.0.
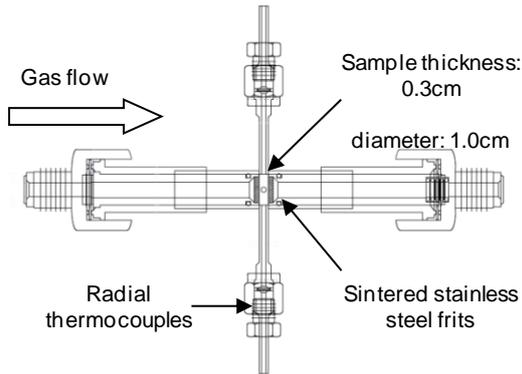

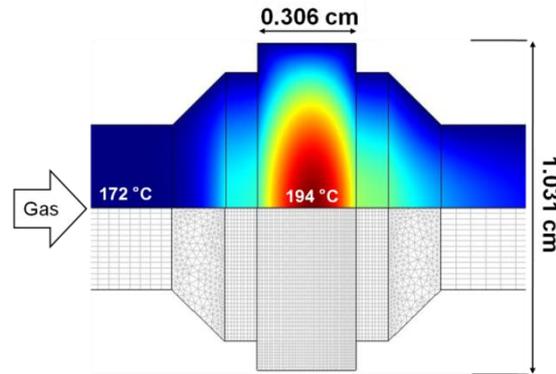Figure 2. The permeability model validation hardware

Figure 3. Axisymmetric FE model geometry and calculated exotherm due to oxidation reaction.
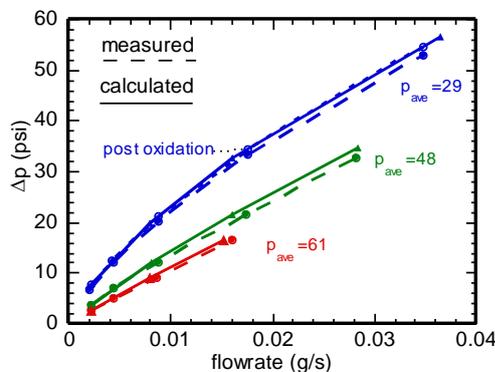

Figure 4. Experimental pressure drop and resulting permeability model parameter fit
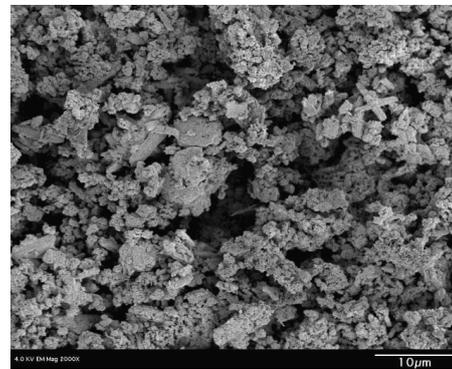

Figure 5. SEM of the 80% porous alane bed

3.2 Chemical kinetics parameters

Alane samples of approximately 90mg were compacted to 80% porous (20% dense). The samples were installed in the flow through sample holder (Figure 2) and integrated with the flow manifold. Prior to each oxidation kinetics experiment, permeability measurements were performed along with a full desorption of the AlH_3. The sample holder was then held at constant temperature while dry air was allowed to flow through the sample. The resulting temperature and pressure signals were recorded. Oxidation experiments at three different temperatures, 76, 172, and 233 °C, were used to determine the temperature dependent coefficients in the chemical kinetics model.

Initial simulations indicated good agreement in overall amplitude of the temperature excursion observed during oxidation yet lacked accuracy in the rate of heating and cooling. This was resolved by directly measuring the oxygen concentration during initial exposure. It was found that the flow mixture was more accurately represented as an ArcTan function that parameterizes the rise rate and steady oxygen concentration rather than an instantaneous step function (Figure 6).

Utilizing the data describing the thermal response at each oxidation temperature, a set of parameter values was assembled that had the highest quality of fit for all of data. Measured and calculated temperature excursions during oxidation are shown for the experiments performed at an initial temperature of ~172 °C in Figure 7. Experimental data is shown as dashed lines while the calculated results are shown as solid lines. The temporally varying temperatures shown are located at three different spatial locations; the wall, the mid-radius, and the center of the bed. The temperature excursion may be quantified by two characteristics, the amplitude of the temperature rise above the

initial temperature, and the shape of the excursion versus time. The degree of fit between the measured and calculated results was similar for each of the three cases.

The experiment at 76 °C (not shown) resulted in a temperature excursion of approximately 9 °C. The validation experiment at 172 °C, Figure 7, resulted in a temperature excursion of approximately 50 °C. The validation experiment at 233 °C (not shown) resulted in a temperature excursion of nearly 60 °C. In each case, the parameter fit process resulted in an accurate representation of the oxidation event. The resulting set of chemical kinetic parameters is shown below along with a summary of results for the temperature excursion amplitude (ΔT), the overall mol fraction of aluminum oxidized (ΔAl), and the rise time for the oxygen concentration (t_{ss}) in each experiment in Table 1.

$$\sqrt{K}k_0 = 6.854e-12,$$
$$k_1 = 1200000,$$
$$Q = 1.73e11,$$
$$Q1 = 1.66e11,$$
$$\alpha = 1,$$
$$D = 150nm$$

Experiment	T (C)	ΔT (C)	ΔAl(%)	t_{ss}(s)	ϕ
5-2-08	76	8	0.07	23	0.692
5-22-08	172	50	0.20	10	0.755
6-3-08	233	54	0.35	30	0.682

Table 1. Summary of results from kinetics parameter fit
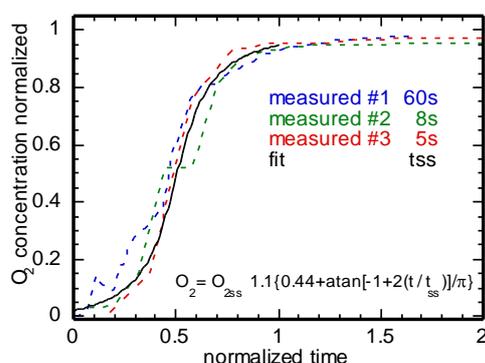
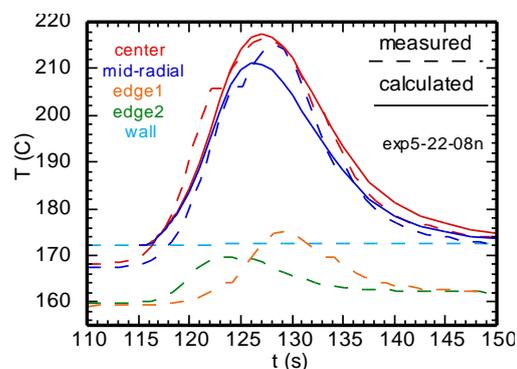Figure 6. Gradual rise in the oxygen concentration as measured at the bed inlet.

Figure 7. Exotherm and resulting parameter fit of oxidation at 172 °C

The calculations described above indicated that very little aluminum oxide is formed at these temperatures. In fact, the oxide mol percent was calculated to be between 0.07 and 0.35 mol%. Measurements using X-ray diffraction (2-theta Scintag XDS 2000) did not indicate any detectable oxide layer – which is consistent with the small amount of oxide present. Measurements using NMR were performed on the un-oxidized and oxidized samples at Caltech. Although definitive depths are difficult to measure, this technique allows for an estimation of the aluminum oxide present. All powder samples were hand mixed with quartz glass powder to make a 1:3 mixture and packed in a zirconia NMR sample tube inside of an Ar-filled glove box. The Al metal, in particular, had to be diluted in order to spin the sample inside of a magnet. A short RF pulse of 0.3 μs corresponding to < π/18 pulse was used to perform ^{27}Al MAS NMR and the sample was spun at 13 kHz. The relative ratios of Al(M) vs oxide layers, and Al(M) vs AlH$_3$ were obtained from integration of Al NMR signals. The oxide layers of the 76 °C sample appear to contain γ-Al$_2$O$_3$ phase and some aluminum oxide in pentacoordination (~33 ppm range) corresponding to estimations as high as 7 mol%. The 172 °C sample measurement indicated oxides in excess of 22 mol% with slightly higher octahedral aluminum sites present (peak at near ~0 ppm). While an explanation of the discrepancy between the calculated values and the NMR results is currently undeveloped, the detection of oxide layers present improves our confidence in the shrinking core oxidation model.

3.3   Model Parameter Sensitivity Studies

Sensitivity studies of the model parameter fitting indicate the relative quality of the determined parameters. Using the 172°C oxidation parameter fit experiment (5-22-08 in Table 1), sensitivity to pore diameter, thermal conductivity, and kinetic parameters were investigated. Figure 8 shows the sensitivity to the pore diameter, indicating a relatively high confidence in the fit of 2.7μm. This is corroborated by Figure 9 that indicates a good, albeit empirical, correlation between pore diameter and porosity. The chemical kinetics sensitivity study (Figure 10) indicates reasonable confidence in the parameter fit. The amplitude of the exotherm and the peak location are influenced significantly by these parameters indicating that an exclusive set can exist for this chemical kinetics model. The thermal response of the sample during oxidation that is the basis for our parameter fitting depends on both chemical kinetic parameters and thermal conductivity. Unfortunately, Figure 11 shows that the results are very sensitive to thermal conductivity. This indicates that this parameter must be accurately measured to isolate conduction heat transfer from chemical kinetics effects, thereby insuring our kinetic parameters are properly quantifying the reaction rates. To address this, future work will improve confidence in the thermal conductivity estimate to insure validity.
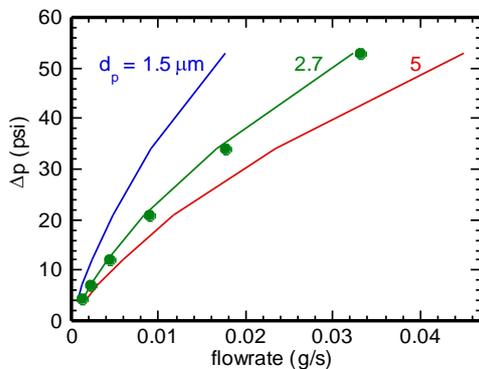
Figure 8. Model shows good sensitivity to pore diameter
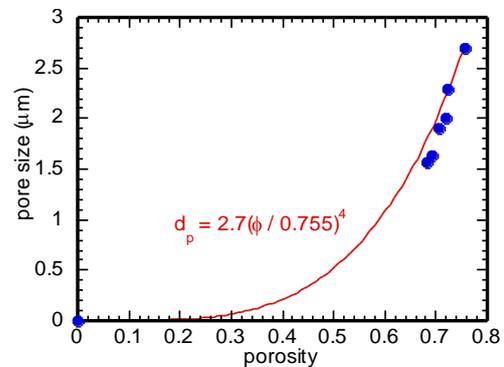

Figure 9. Pore diameter fit for a variety of samples indicates good correlation to bed porosity
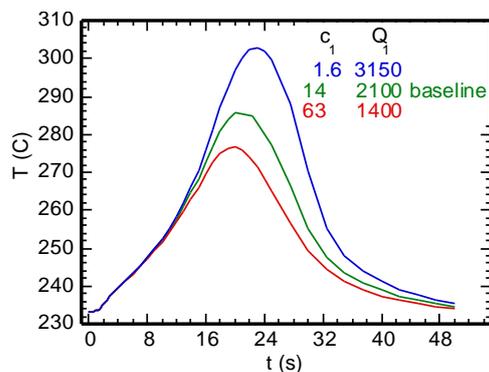

Figure 10. Chemical kinetics parameters indicate a change in amplitude and shape of the exotherm indicating high confident in the quality of the fit
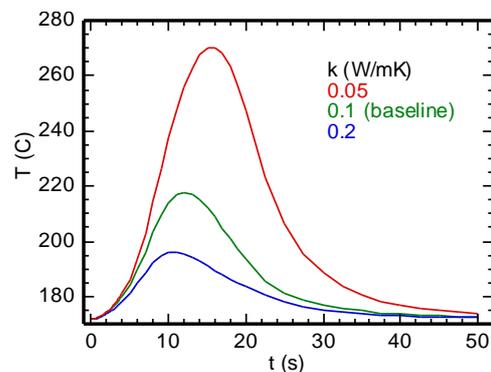

Figure 11. The exotherm is highly sensitive to the thermal conductivity and indicates that direct measurement of the property should be performed

4.0 SIMULATION OF SCALED-UP CONTAMINATION PROCESSES

To address the breach-in-tank contamination scenario, we assembled a finite element model of a dead-end stainless-steel cylindrical vessel with an inlet/outlet stem on one end. The axisymmetric model was built using Comsol™ Muliphysics. The chemical kinetics and permeability models described above for the alane bed were used. The model geometry is a cylinder 0.3 m in length and 0.0254 m in diameter with a 2 mm wall thickness as shown in Figure 12. Simulations were performed with and

without heat losses to the environment, as given by $q = h_w(T_\infty - T_w) + \varepsilon\sigma(T^4 - T_w^4)$, where T_∞ is the ambient temperature and T_w is the local wall temperature of the vessel. Three cases were considered, a 'no-insulation' case with $h_w = 11$ W/m^2-K (natural convection) and $\varepsilon = 0.3$, a 'partially insulated' case with $h_w = 5.5$ and $\varepsilon = 0$, and a 'perfectly insulated' case with $h_w = \varepsilon = 0$. Porosity was varied between 0.5 and 0.76. The initial temperature and pressure were set to 150 °C and $1.01\cdot10^5$ Pa, respectively. The boundary conditions applied to the stem were a pressure of $1.01\cdot10^5$ Pa for the momentum equation, a temperature of 25 °C for the energy equation, and an oxygen concentration of 8.56 mol/m^3 (air) for the species transport equation.
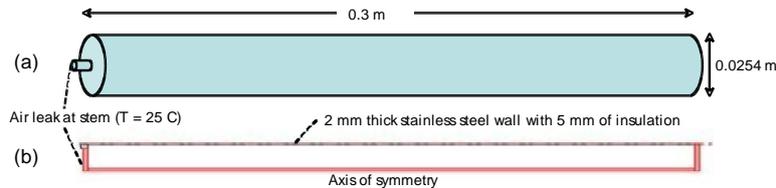
Figure 12. The geometry assumed to be representative of an alane hydrogen storage tube with a single inlet/outlet stem for automotive applications. (a) Schematic, (b) axisymmetric FEM model

Figure 13 shows six snap-shots in time of the thermal state of the alane cylinder during the contamination process where the cylinder is partially insulated and at the alane has a porosity of 0.755. A reaction front propagates through the bed with maximum temperatures of approximately 200 °C at around 60 seconds. This is more easily observed in Figure 14 where the axial temperature profiles are shown for the same time states. In general, a reaction zone propagates along the entire length of the bed with the exothermicity and extent of the reaction competing with the loss of heat to the environment. The temperature is a maximum within the reaction zone, but overall the temperature decreases with time due to the environmental losses.
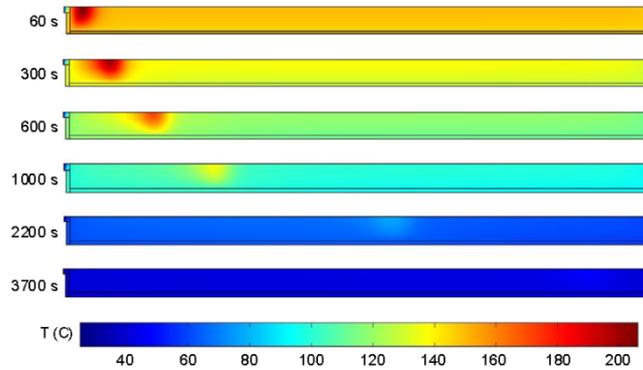

Figure 13. Results for the breach-in-tank scenario simulation for the 80% porous bed indicates a reaction front propagating though the system for 1 hour.

The axial gas velocity profiles are shown in Figure 15. This induced gas velocity is driven by a complex interplay between gas diffusion, consumption of oxygen in the reaction zone, and cooling of the gas due to environmental losses. Initially, oxygen diffuses into the cylinder while some of the inert gas originally in the cylinder diffuses out. The oxygen is consumed in the reaction zone, which results in a zone of reduced pressure and a pressure gradient. This pressure gradient results in the flow of gas towards the reaction zone from both the left and the right at early times, as indicated by positive velocities for z < 1 cm and negative velocities for z > 1 cm at 60 s. At later times the pressure inside the cylinder to the right of the reaction zone has been sufficiently reduced to result in positive velocities everywhere. The velocity is largest near the stem, and then decreases as the gas flow spreads out over the cross section of the cylinder. It remains large up to (the left of) the reaction front where the oxygen is consumed, and then drops precipitously past (to the right of) the reaction zone where it

is driven only by the continuous cooling of the gas due to environmental losses and the reduction in gas pressure that this causes. At still later times the temperature approaches that of the ambient and the reaction rate decreases. Gas continues to flow into the cylinder until the gas pressure approaches the ambient value (one atmosphere) and then the gas velocities tend toward zero.

Figure 16 shows the axial oxygen concentration profiles. The transport of oxygen into the bed is driven by both advection and diffusion. The concentration is largest at the stem and decreases towards zero at a point to the right of the reaction zone, i.e. the oxidation process consumes all of the oxygen during the early times while temperatures are still large. At late times (not shown) the cylinder is filled with oxygen at near the ambient concentration, however very little additional oxidation occurs due to a combination of the reduction in temperature resulting from environmental losses and the passivation of the alane by the oxide layer that forms around all of the particles. The axial aluminum deficit profiles are shown in Figure 17. The profiles sweep out an overall enveloping profile that is largest near $z = 1$ cm where the largest temperature occurred (which occurred at 60 s). The amount of aluminum that is oxidized is very small, ranging from 0.03 to 0.23%.
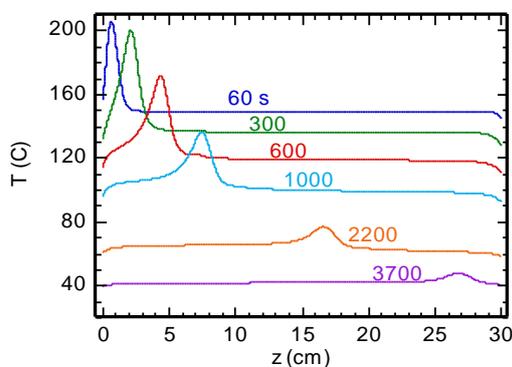

Figure 14. Thermal response of the partially insulated case as a function of length and time
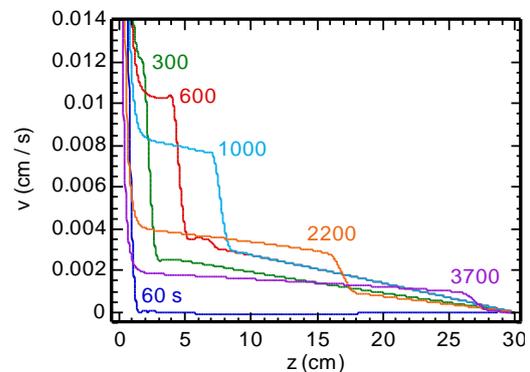

Figure 15. Velocity of the gas entering the bed as a function of length and time
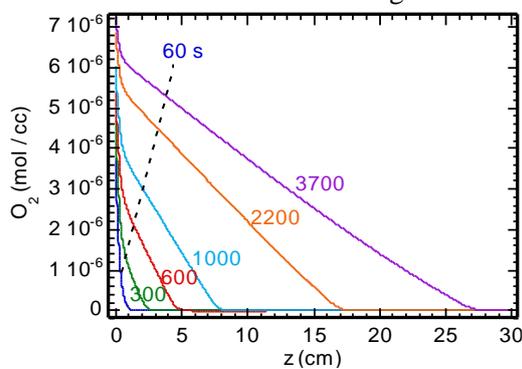

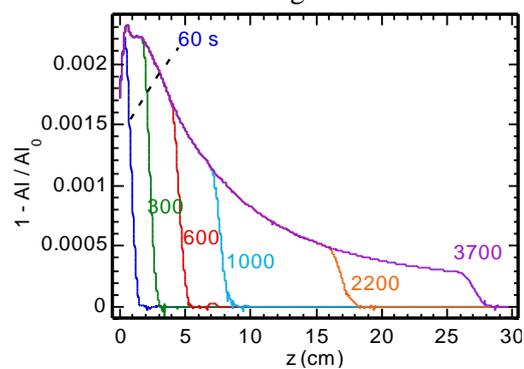Figure 16. Oxygen concentration as a function of length and time

Figure 17. Amount of aluminium consumed in the reaction as a function of length and time

To investigate the influence of heat loss and packing density on the reaction front characteristics, it is helpful to define a reaction zone and its associated temperature and velocity. The *reaction zone temperature* is the temperature maximum associated with the exotherm. The *reaction zone velocity* is the rate of change of the location of the temperature maximum.

First, considering the impact of insulation for a porosity of 0.76, perfect insulation results in the highest reaction zone temperature as shown in Figure 18, as might be expected. Interestingly, the reaction zone velocity decreases with increased insulation and temperature, as shown in Figure 19. This is due to the kinetics of the reaction and the oxygen transport into the cylinder. As described in Section 2.2, the amount of aluminum that participates in the oxidation process increases with temperature. Meanwhile the transport of oxygen into the cylinder is limited by the small opening in the stem. Thus, as the amount of aluminum available increases it takes more time to consume it, which

slows the rate of movement of the reaction zone. That is, the reaction zone velocity is determined by the amount of available aluminum and the limited transport rate of oxygen into the bed.

To investigate the impact of higher densities on the reaction processes, we consider a partially insulated system at 0.5 porosity as might be more appropriate for engineered systems. The properties for this case, were calculated based on the thermal conductivity model and the empirical pore size model (Figure 9). These result in a large effective conductivity and a smaller pore size for the bed. The resulting reaction zone temperature is shown in Figure 20, where it is compared to the 0.76 porosity case. The lower permeability for $\phi = 0.5$ reduces the diffusion of oxygen gas, and the larger conductivity increases heat losses resulting in lower temperatures compared to the 0.76 porosity case. Interestingly, the impact on reaction zone velocity (Figure 21) is reversed compared to the insulation analysis; in this case, lower temperatures result in lower reaction zone velocities. However, the same mechanism that reduced the reaction zone velocity when the insulation was increased is at play when the packing density is increased, i.e. an increase in the amount of available aluminum. In the former case the amount of available aluminum increased due to a larger temperature, while in the latter case the larger packing density itself results in more available aluminum, in spite of the reduction in reaction zone temperature seen in Figure 20.

The alane system has provided a unique opportunity to observe the propagation of a reaction front through a hydrogen storage bed during a breach in tank scenario. Considering the alane system, the hazard presented by the propagating reaction front is low, resulting in only a moderate exotherm. Other, more reactive systems may result in a more significant hazard where, if un-mitigated, the breach-in-tank could lead to an over-temperature event causing containment vessel failure or other unfavorable outcomes. Future efforts will consider the behavior of complex metal hydrides to quantify the breach-in-tank reaction processes for alkali-metal containing classes of systems.
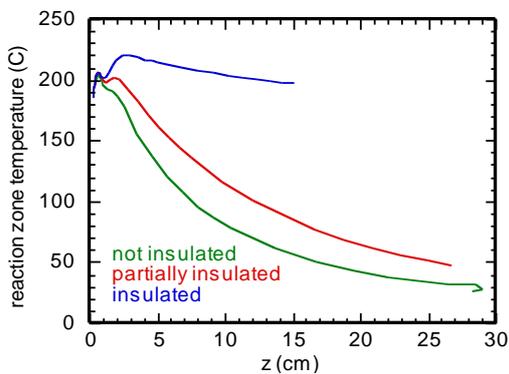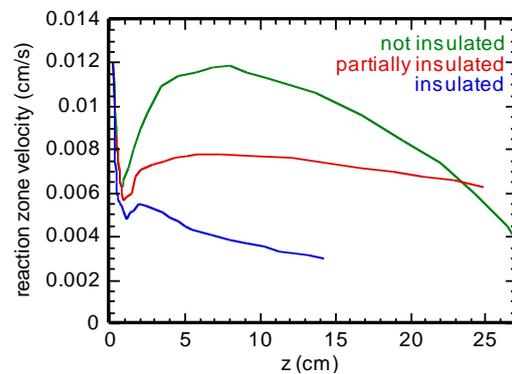
Figure 18. Reaction zone temperature as a function of insulation degree and bed length

Figure 19. Reaction zone velocity as a function of insulation degree and bed length
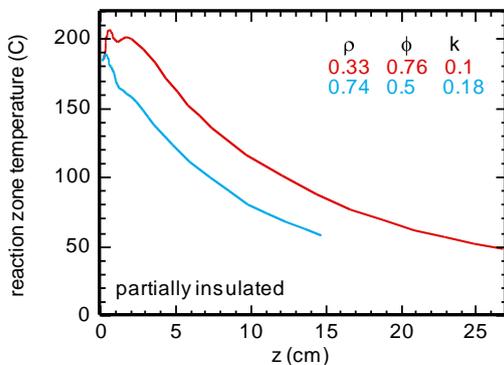
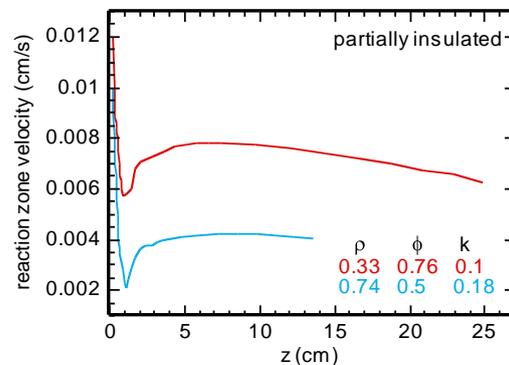Figure 20. Reaction zone temperature for the 0.5 porosity case in contrast to the 0.76 porosity case

Figure 21. Reaction zone velocity for the 0.5 porosity case

5.0 CONCLUSIONS

A breach in tank contamination event of an alane containing system results in a moderate temperature reaction front that progresses through the entire system. The extent of reaction is controlled by the rate of heat loss from the system. Higher density systems actually improve the scenario, despite the presence of more fuel per unit volume. This is due to the impact of low permeability on the reaction front propagation rate. In general, the processes we predict to occur fall well within the parameter space from which we built the chemical kinetics models. It should be noted that kinetics are unknown for temperatures exceeding approximately 400 °C. If a scenario resulted in calculated temperatures above this temperature, less confidence in the results would be ascribed – especially as the temperatures approach the melting point of aluminum. Future efforts will focus on the validation of scaled-up predictions for alane and other more complex hydrogen storage materials. The methods used to develop the models described here are appropriate for a variety of solid state hydrogen storage materials and systems. These methods and resulting models can be used to develop safe system design guidelines for systems, and identify methods for mitigating hazards presented by hydrogen storage system life-cycle events.

REFERENCES

1. Sandrock, G. "A panoramic overview of hydrogen storage alloys from a gas reaction point of view". Journal of Alloys and Compounds 293 –295 (1999) 877 –888

2. International Energy Agency Hydrogen Implementing Agreement, 2007 Annual Report on the Production and Utilization of Hydrogen. Edited by M. Valladares, 2007, www.ieahia.org

3. Khalil, Y.F. and Mosher, D.A. "Risk Quantification of Hydride Based Hydrogen Storage System for Automotive Applications ", Proceedings from the ICHS 2009 ICHS, Corsica, Fr. In press.

4. Graetz, J. and Reilly, J. "Decomposition kinetic of the AlH3 polymorphs" J. Phys. Chem. B 109 (2005) 22181-22185

5. Herley, P. J.; Irwin, R. H. "A preliminary study of the thermal and photolytic decomposition of aluminium hydride powder", J. Phys. Chem. Solids 39, (1978) 1013.

6. Herley, P. J.; Christofferson, O.; "Decomposition of α-aluminum hydride powder" Irwin R. J. Phys. Chem. 85 (1981) 1874.

7. Herley, P. J.; Christofferson, O. "Decomposition of .alpha.-aluminum hydride powder." J. Phys. Chem. 85 (1981) 1887.

8. Graetz, J and Reilly, J; "*Thermodynamics of the polymorphs of AlH3*", Journal of Alloys and Compounds 424 (2006) 262–265

9. Bazyn, T.; Eyer, R.; Krier, H.; Glumac, N. "Combustion characteristics of aluminium hydride at elevated pressure and temperature", J. Propulsion Power 20 (2004) 427.

10. Weiser, V et al. "On the Oxidation and Combustion of AlH3 a Potential Fuel for Rocket Propellants and Gas Generators", Propellants, Explosives, Pyrotechnics 32 (2007) 213.

11. JB Young and B Todd; Intl J Heat and Mass Transfer, 48 (2005)

12. Rodriguez-Sanchez, A. et al. **'**Expanded graphite as heat transfer matrix in metal hydride beds". International Journal of Hydrogen Energy 28 (2003) 515 – 527

13. Frank M. White, 'Viscous fluid flow', McGraw Hill, New York, 3rd Edition, (2006).

14. A. F. Mills, 'Mass Transfer', Prentice Hall, Upper Saddle River, NJ, 2nd Edition, (2001).